Pol. J. Environ. Stud. Vol. XX, No. X (XXXX), 1-15
DOI: *10.15244/pjoes/235734* ONLINE PUBLICATION DATE: 2026-11-03

Original Research

In-situ Methanation of Carbon Dioxide Fixed in the Pores of the Adsorbent Material

Lenka Polívková*, Karel Ciahotný, Tomáš Hlinčík, Veronika Kyselová

University of Chemistry and Technology, Prague; Department of Sustainable Fuels and Green Chemistry; Technická 5, 166 28 Prague 6 – Dejvice, Czech Republic

Received: 26 February 2026
Accepted: 27 August 2026

Abstract

The methanation of carbon dioxide via its reaction with hydrogen has recently become a widely studied topic. This process is typically investigated in a flow system with a catalyst placed in a catalytic reactor through which a mixture of reactant gases (carbon dioxide and hydrogen) flows. In contrast, this study investigates a batch reactor concept, where carbon dioxide is adsorbed within the porous structure of the catalyst and hydrogen is subsequently introduced. The novelty of this research lies in the technological arrangement of the process, in which a single material simultaneously acts as both adsorbent and catalyst within one reactor, enabling alternating CO_2 adsorption and its subsequent methanation. The central component is therefore an adsorbent for carbon dioxide capture that also serves as a catalyst for its conversion into methane. A system based on this principle can therefore be used both for capturing carbon dioxide from various gas mixtures with recovery in purified form and for its conversion into synthetic methane, provided a sufficient supply of hydrogen is available. This research confirms that the investigated single-reactor methanation approach using one material that functions both as adsorbent and catalyst is fully operational and suitable for further testing at the pilot scale.

Keywords: carbon dioxide, adsorption, methanation, synthetic methane

Introduction

The development and deployment of CCUS (Carbon Capture, Utilization and Storage) technologies have become a major focus of scientific and industrial interest in recent years, offering a promising pathway to reduce anthropogenic CO_2 emissions. In the European Union, the option of underground storage of CO_2 captured from various industrial gas streams was suspended more than a decade ago, which has shifted considerable attention to its utilization or conversion into value–added products [1]. A frequently investigated route is the hydrogenation of carbon dioxide to methane, commonly known as the Sabatier reaction, which involves the catalytic reduction of carbon dioxide with hydrogen to produce methane and water [2-6]. Nickel–based catalysts are the most commonly used for this methanation reaction; however, catalysts based on copper, cobalt, ruthenium, or rhodium have also been explored [7-25]. The methanation of carbon dioxide typically occurs within a temperature range of 125-675ºC. Higher yields are generally obtained at temperatures exceeding 145ºC, with maximum

*e-mail: Lenka.Polivkova@vscht.cz
Tel.: +420 220 444 230
0000-0002-5600-8058

© 2026 This article is licensed under a Creative Commons Attribution-NonCommercial 4.0 International (CC BY-NC 4.0)

reaction rates and the highest selectivity observed between 325 and 425ºC [6, 26]. At temperatures above 475ºC, the formation of carbon monoxide increases due to the endothermic Reverse Water Gas Shift (RWGS) reaction [27].

One of the viable approaches to remove carbon dioxide from combustion gases and industrial waste streams is its capture using suitable adsorbents that exhibit high affinity for CO_2 [28, 29]. These adsorbents are characterized by a well–developed porous structure that features a high pore volume and a large internal surface area. If catalytically active species are appropriately incorporated into such materials, they may also serve a dual function as catalysts. An adsorber packed with such an adsorbent can, in the first step, capture CO_2 from a gas mixture, and subsequently, upon introduction of hydrogen into the surrounding environment, operate as a stationary catalytic reactor allowing the conversion of sorbed carbon dioxide to methane. Therefore, this concept can be described as an adsorptive–catalytic system, which can flexibly provide either a carbon dioxide–enriched gas or a methane–rich product gas, depending on operating conditions [30-37]. The present study investigates this integrated pathway.

Bifunctional materials (BFMs) for CO_2 adsorption and subsequent methanation represent a significant advancement in carbon capture and utilization (CCU) technologies. These materials incorporate dual functionalities: they both capture CO_2 from gaseous streams and catalyze its conversion to methane by hydrogenation. This integrated approach improves the efficiency of carbon resource utilization, paving the way for sustainable synthetic natural gas production [34-39].

CO_2 methanation with hydrogen is used on an industrial scale when hydrogen produced by water electrolysis powered by surplus electricity from the distribution grid is available. Such surpluses are typically available only for limited periods and cannot be reliably predicted in advance. Consequently, the actual operating time of the unit cannot be determined beforehand; rather, its operation is expected to be controlled according to the current situation in the electricity distribution network. In the case of frequent shutdowns, a technology based on batch reactors is more suitable, as the reaction time required for methanation can be adjusted to the specific operating conditions. In addition, when hydrogen is not available, the unit can alternatively be used solely for CO_2 adsorption from gases and for the production of pure CO_2. This can improve the payback period of the investment.

In general, the synergistic design and application of BFMs for CO_2 capture and methanation represent a promising avenue to advance carbon–neutral fuel technologies. By elucidating their mechanisms and optimizing the material composition, a further contribution to mitigating the effects of climate change can be achieved.

From an industrial perspective, this system can be implemented in any setting where a waste gas stream containing a sufficient concentration of carbon dioxide is available (e.g., flue gases from fossil fuel or biofuel combustion), along with a source of hydrogen production (e.g., electrolyzers utilizing surplus electricity from power grids). The methane produced in such a system can serve as a dispatchable energy source, particularly in situations where the electricity demand exceeds the supply and additional generation is required. Therefore, the system can be viewed as a backup method for electricity production without introducing additional CO_2 emissions into the environment. An important advantage of this concept lies in its product flexibility, as the system can be tuned to deliver different outputs. The first potential product is captured carbon dioxide, which can be stored underground in gaseous, liquid, or supercritical form [40]. The second product is methane, which is often used for short–term peak electricity generation because of its favorable combustion characteristics and rapid response capabilities.

To enable the production of methane from CO_2, a sufficient supply of green hydrogen, produced through water electrolysis powered by renewable energy sources, is required. In recent years, the Czech Republic has seen the first installations of electrolyzers designed to utilize surplus electricity generated during periods of overproduction of renewables. This excess electricity is often available at negative market prices, which has a significant impact on the overall cost of hydrogen production [41-47].

However, surplus electricity in power grids is typically available only for relatively short periods (currently amounting to several hundred h per year in the Czech Republic), which limits the operational time window for hydrogen production. In this context, methane storage offers several advantages over hydrogen storage. Methane possesses an approximately three times higher volumetric energy density than hydrogen, meaning that only about one third of the storage volume is required to store the same amount of energy. Safety considerations also play a critical role: methane exhibits significantly narrower explosion limits, making it considerably less prone to explosion hazards than hydrogen. Furthermore, gas engines or turbines powered by methane combustion generally achieve higher thermodynamic efficiency than equivalent systems powered by hydrogen combustion products [48].

Methanation of Carbon Dioxide with Hydrogen Using Adsorbed Carbon Dioxide

The catalytic conversion of carbon dioxide to methane via its reaction with hydrogen was first discovered in 1902 by the French chemist Paul Sabatier; accordingly, this process is often referred to as the Sabatier reaction after its discoverer. For this discovery, P. Sabatier was awarded the Nobel Prize in Chemistry in 1912.

This process can be simply represented by the following equation:

$$CO_{2(g)} + 4H_{2(g)} \leftrightarrow CH_{4(g)} + 2H_2O_{(g)}$$
$$\Delta H_{298.15} = -165.0 \text{ kJ mol}^{-1} \quad (1)$$

This is an exothermic reaction that releases a significant amount of heat into the surroundings. In the technological process, this heat can be used to heat the adsorbent saturated with CO_2 to the reaction temperature required for methanation.

The actual mechanism of this reaction is relatively complex, and various theories regarding the formation of methane through hydrogenation of carbon dioxide are reported in the scientific literature. One theory proposes that CO_2 is first converted to CO, which is subsequently methanated to CH_4. Another theory assumes a direct hydrogenation of CO_2 to CH_4 without the formation of CO as an intermediate [49].

In his early experiments, P. Sabatier used nickel as the catalyst. The reaction temperature required when using a nickel catalyst typically starts at approximately 125ºC. Various porous materials have been tested as catalyst supports, such as γ–Al_2O_3, TiO_2, SiO_2, ZrO_2, and CeO_2 [50, 51].

Other metals have also been tested as catalysts, including Ru, Rh, Co, Fe, and Mo. Among the most active catalysts are nickel, ruthenium, and rhodium. However, the latter two metals are significantly more expensive than nickel [50].

Nickel stands out among all catalysts due to its high selectivity for converting CO_2 to CH_4, whereas other catalysts tend to produce significant amounts of higher hydrocarbons. The share of these hydrocarbons is influenced by reaction conditions, mainly the residence time of the reactants in the catalytic reactor; longer residence times increase the proportion of higher hydrocarbons among reaction products [51-53].

By investigating variations in reaction rate and activity across temperature, pressure, and reaction time parameters, optimal reaction conditions can be identified to improve both reaction efficiency and economic viability [53-56].

Research indicated that the rate of CO_2 methanation is more influenced by the partial pressure of H_2 than that of CO_2, particularly at lower levels of CO_2 conversion. In a study by Champon et al. [57], the relationship between the rate of CO_2 methanation and the partial pressures of reactants and products was delineated at varying temperatures using the Ni/Al_2O_3 catalyst dispersed in SiC. Their findings underscored a strong dependence of CH_4 formation on H_2 concentration at a CO_2 partial pressure of 22 kPa while indicating a lesser impact of CO_2 (at 55 kPa H_2) and CH_4 pressures. The partial pressure of water showed an obvious inhibitory effect.

Exceeding the upper temperature limit (700ºC) of the recommended range significantly affects the methane yield due to the thermodynamic equilibrium of the reaction and the fact that methanation catalysts at high temperatures catalyze the reverse reaction of methane with steam, producing CO and hydrogen. This process is used industrially to produce synthesis gas from natural gas. Higher reaction pressures have a favorable effect on CO_2 methanation (five volumes of reactants produce three volumes of products) [51].

The Sabatier reaction requires a large excess of hydrogen (for complete conversion of one volume of CO_2, four volumes of hydrogen are needed). From an economic perspective, it is therefore important that the hydrogen used in the reaction has the lowest possible cost, since only half of it is converted into the desired product (methane). The other half of the hydrogen used in the reaction is converted into water.

The low temperatures required to initiate the Sabatier reaction led us to the idea of methanation of CO_2 adsorbed from waste gases on the surface of a suitable adsorbent if a sufficient amount of hydrogen is supplied nearby. CO_2 is retained within the porous structure of the adsorbent through physical adsorption. This process is influenced by the specific conditions under which it takes place. As temperature increases and partial pressure decreases, the CO_2 adsorption capacity of the adsorbent decreases. Methane is also retained within the porous structure of the adsorbent by a similar mechanism.

However, the adsorbent must contain a suitable catalytic element on its surface, preferably Ni. After saturating the adsorbent with CO_2 and subsequently filling the adsorber with hydrogen, it is possible to heat the adsorber/reactor to the desired reaction temperature appropriately. Once the methanation reaction starts, the adsorbent continues to heat up as a result of the released reaction heat, which is not removed from the reactor. In the case of a significant temperature increase in the reactor, the generated reaction heat can be removed by means of a suitable heat transfer medium to another reactor, thereby heating its contents to the required reaction temperature. During system startup, an external energy source, such as steam with appropriate parameters, will be needed to heat the reactor to the desired temperature.

After completion of the methanation reaction, when the reactor temperature no longer rises and the pressure in the reactor no longer decreases, it is necessary to cool down the catalytic bed and the products contained in the reactor and then discharge them from the reactor. Upon reaching the temperature required to start the next operating cycle, the reactor can be reused to capture another amount of CO_2 and subsequently perform another methanation step.

Materials and Methods

The possibility of methanizing CO_2 adsorbed on the surface of a suitable adsorbent in a batch reactor using hydrogen was investigated in a laboratory experimental setup. To more thoroughly assess the methanation

of CO_2, a series of experiments was conducted using model gases (CO_2 and H_2). The results obtained allowed evaluation of the proposed principle of this methodology and determination of the specific operating conditions of the apparatus (optimal catalyst type, required temperatures, reaction times, and partial pressures of the gases used) to achieve the highest possible efficiency in converting CO_2 to methane. The aim of the experiments was to identify the specific reaction conditions under which the methanation reaction proceeds with the highest possible efficiency. Additionally, the results served as a basis for conducting the next testing phase of the proposed technology using a larger pilot unit and real gases (flue gases from coal and biomass combustion). Experiments using this unit are planned to investigate the long-term stability of the adsorbents/catalysts under real flue gas conditions, as impurities present in these gases may lead to their deactivation.

Preparation of Adsorbent/Catalysts

Two types of adsorbent/catalysts were prepared for experimental testing. Nickel (Ni) was chosen as the catalyst, as it demonstrated the best catalytic activity among all active elements tested in previous experiments [51] conducted using a flow catalytic reactor.

The selection of suitable adsorbents, which also served as supports for the catalytically active element (Ni), was based on the following criteria:

- Minimum specific surface area: 150 $m^2\ g^{-1}$
- Minimum adsorption pore volume: 0.2 ml g^{-1}
- Minimum adsorption capacity of the material for carbon dioxide at atmospheric pressure and room temperature: 10%
- Minimum average mechanical strength of particles under pressure: 90 N per particle

Material Based on γ–Alumina Impregnated with Nickel

For testing, boehmite in the form of hollow cylinders with a length of 6 mm and a diameter of 5 mm was used. It was calcined in a muffle furnace at a temperature of 500ºC for 3 h (heating rate was 5ºC min^{-1}). During calcination, boehmite recrystallized into γ–alumina. Subsequently, the γ–alumina was impregnated with a 20% solution of nickel nitrate, with a soaking time of 1 hour. After impregnation, the γ–alumina was filtered from the solution and placed into a muffle furnace preheated to 500ºC (heating rate 5ºC min^{-1} and soaking time 3 h). At this temperature, the impregnated nickel nitrate decomposed into nickel oxide and nitrogen oxides. This impregnation with a 20% nickel nitrate solution was repeated 5 times in total. This procedure ensured a uniform distribution of NiO without the formation of large surface agglomerates, and repeating this process increased the metal loading on the material.

Material Based on Envisorb B+ Impregnated with Nickel

The Envisorb B+ adsorbent, containing approximately 85% SiO_2 and approximately 15% activated carbon, was supplied by Engelhard Process GmbH in the form of black spheres with a diameter of 2-5 mm. Envisorb B+ was impregnated with a 20% nickel nitrate solution in the same manner as the γ–alumina–based material.

Before using these materials in methanation experiments, it was necessary to activate the catalyst by reducing the catalytically inactive NiO to the catalytically active Ni form. The reduction was carried out directly in the methanation reactor under a pure hydrogen atmosphere at a pressure of 1 MPa and a temperature of 500ºC for 3 h.

Determination of the Elemental Composition of Adsorbent/Catalysts

The carbon, nitrogen, hydrogen, and sulfur contents in the adsorbent/catalyst were determined by elemental analysis using a Flash 1112 instrument (Thermo Scientific). The elemental composition of the analyzed samples was calculated from the composition of gases produced by combustion of the sample in an oxygen stream at high temperature. The main components of the gases were separated on a chromatographic column and subsequently detected by a thermal conductivity detector. Quantitative determination of components was performed by burning a standard with a precisely known composition under the same conditions as the analyzed samples.

Determination of Nickel Content

The nickel content in the adsorbent/catalyst was determined by X–ray fluorescence analysis (XRF) using a PANalytical instrument. The dried sample was ground and irradiated using an X–ray tube (Rh 60 kV) with variable-wavelength radiation and the fluorescence spectrum was recorded. The intensity of lines with precisely defined wavelengths was proportional to the concentration of the respective element in the analyzed sample.

Determination of Specific Surface Area and Pore Volume

The specific surface area of the samples was measured using a Coulter SA 3100 analyzer (Beckman Coulter). The method is based on the physical adsorption of nitrogen on the internal surface of the sample at 77 K. The samples were degassed under high vacuum at 150ºC for 240 min prior to measurement. The degassed sample was immersed in liquid nitrogen, and precise volumes of gaseous nitrogen were dosed into the measuring cell in steps. After equilibrium was reached at each step,

the equilibrium pressure was measured, and the amount of adsorbed nitrogen was calculated. From these data, an adsorption isotherm (relative pressures from 0 to 0.99 at 77 K) and a desorption isotherm were constructed. The specific surface area of the sample was calculated based on the BET equation (Brunauer–Emmet–Teller). The total pore volume was determined on the basis of the amount of adsorbed nitrogen at a relative pressure close to one.

Determination of the CO_2 Sorption Capacity of the Samples

The sorption capacity of the samples for carbon dioxide was determined using a Quantachrome ASiQ instrument. The samples were tested at temperatures of 40ºC, 60ºC, 80ºC, and 100ºC. The sample weight for the measurement was approximately 0.5 g. The activation of the samples in the measuring cells was carried out by heating to a temperature of 150ºC (10ºC min^{-1}) for 120 min in a nitrogen stream, followed by the evacuation of the measuring cells for an additional 120 min. After activation, weight loss was determined gravimetrically. During measurement, known volumes of a gas mixture containing carbon dioxide (15% CO_2 in N_2) were dosed into the cell with the activated sample at the test temperature. After equilibrium pressure was reached following each dose, the adsorbed amount of CO_2 was calculated. After the adsorption step, regeneration of the sample was carried out in the same way as its activation prior to adsorption (150ºC for 2 h in nitrogen, followed by evacuation for 2 h). The adsorption–regeneration cycle was repeated 3 times.

Description of the Static Methanation Apparatus

The core of the laboratory–scale static methanation apparatus was a high–pressure adsorber/reactor made of stainless steel, cylindrical in shape, with a length of 150 mm, an internal diameter of 30 mm (volume 106 ml), and a wall thickness of 4 mm. The reactor (see Fig. 1) was designed for a maximum pressure of 10 MPa and was sealed at both ends with threaded end caps.

The adsorber/reactor was placed inside a protective stainless–steel housing (protective tube with a diameter of 11.4 cm, a length of 18.5 cm and a wall thickness of 3 mm). Heating/cooling of the reactor was ensured by a flow of hot/cold air introduced between the protective housing and the adsorber/reactor.

The reactor was connected to gas cylinders containing test gases (He, CO_2, H_2) through a gas-tight system of stainless-steel tubing with a diameter of 4 mm and an electronic pressure regulator. The system upstream of the adsorber/reactor was equipped with a manometer and a safety pressure valve (7 MPa). After the experiment, the resulting reaction gases were discharged from the adsorber/reactor through a shut–off valve followed by a needle control valve and a condenser into a RESTEK gas sampling bag intended for gas mixture collection.

The adsorber/reactor was equipped with a thermocouple to measure the temperature of the adsorption/reaction bed. Thermocouple data were recorded 2 times per second.

A schematic diagram of the methanation apparatus is shown in Fig. 2.

Methanation Experiment Procedure

Sample loading: 35 g

Gas specification: He 4.8 (99.998%, SIAD), H_2 3.0 (99.90%, SIAD), CO_2 4.0 (99.990%, SIAD)

The methanation experiments were carried out according to the following procedure. First, the reactor was filled with the tested adsorbent/catalyst and placed in the testing apparatus. The entire system was then purged with helium for 30 min and subsequently pressurized with helium to an overpressure of 3 MPa. After this step, all gas inlet and outlet shutoff valves connected to the adsorber/reactor were closed. During the next 3 h, pressure drops were monitored to identify potential leaks, and if detected, they were located and sealed. Once the system was confirmed to be leak–tight, helium was released and the apparatus was purged with pure carbon dioxide for 10 min.

The adsorber/reactor was then closed at the outlet and pressurized with pure CO_2 to an overpressure of 2 MPa, after which the inlet was also closed. Once the temperature and pressure stabilized within the adsorber/reactor, the outlet valve was opened to release the gas

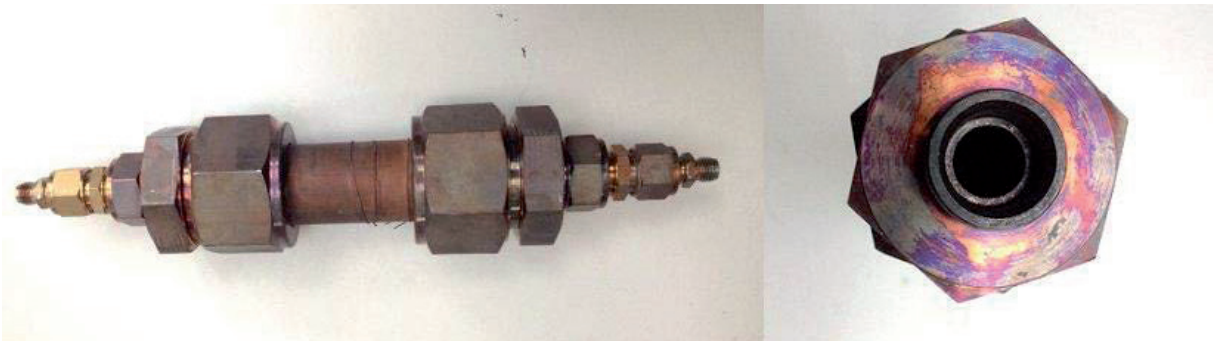


Fig. 1. Photograph of the adsorber/reactor.

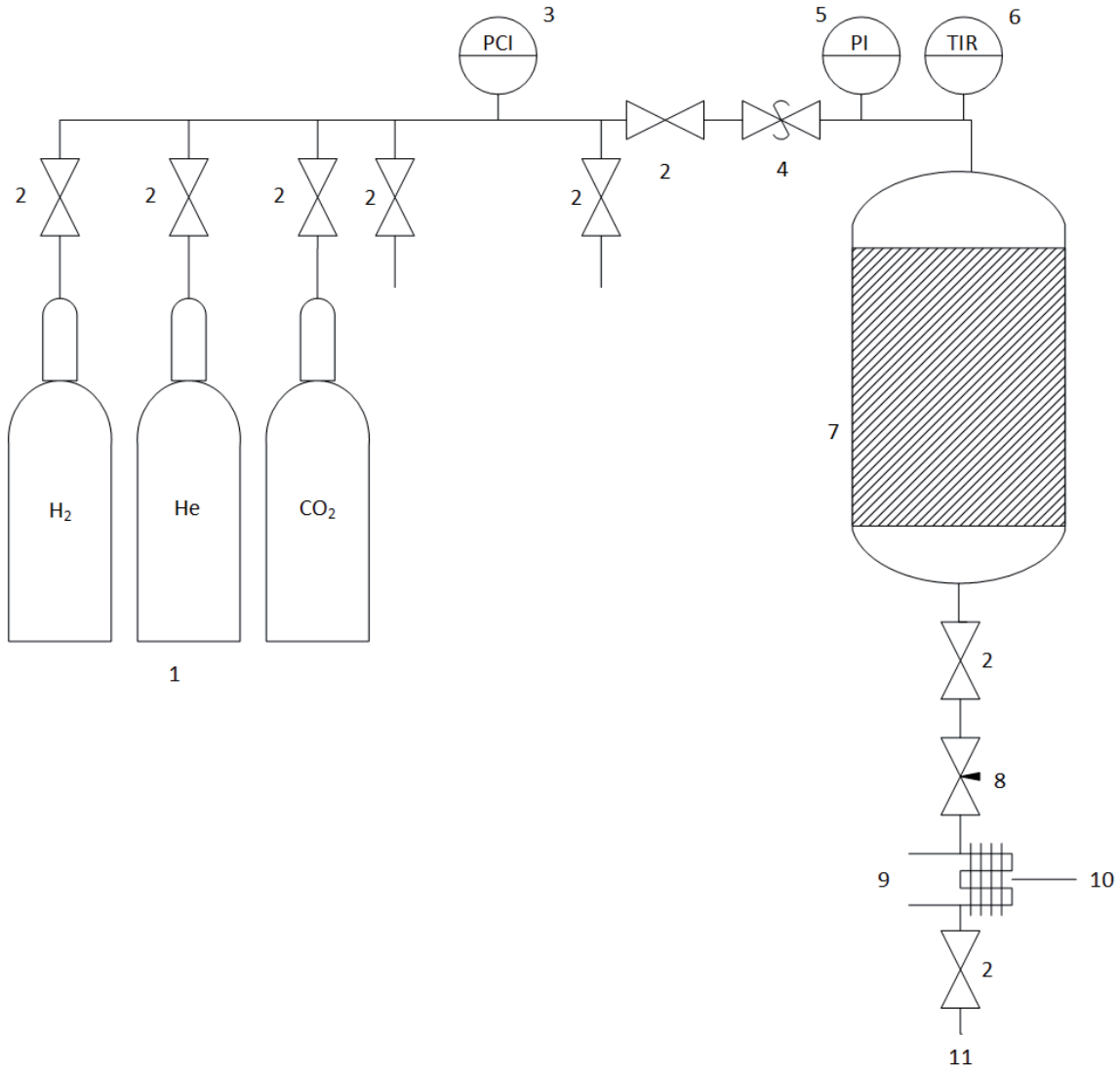


Fig. 2: Diagram of the static methanation apparatus. 1 – gas cylinders; 2 – shut–off valves; 3 – electronic pressure regulator; 4 – safety valve; 5 – manometer; 6 – thermocouple for measuring temperature inside the reactor; 7 – adsorber/reactor with protective housing and indirect heating; 8 – needle control valve; 9 – cooler/condenser; 10 – sampling line for connection to gas sampling bag; 11 – condensate drain.

until the desired CO_2 overpressure remained in the reactor (0.02 or 0.05 MPa). Subsequently, the system was pressurized with hydrogen to the required overpressure (1 or 1.5 MPa), and the adsorber/reactor was sealed. After stabilization of both temperature and pressure inside the reactor, heating with hot air was initiated and the increase in temperature and pressure of the gas mixture was continuously monitored.

When the target temperature was reached, the heating was adjusted to maintain a constant temperature in the reactor for the selected methanation duration, which ranged from 0 to 21 h (where 0 h indicates that the heating was switched off immediately after reaching the desired temperature). After the chosen methanation time had elapsed, the reactor was cooled with cold air (50ºC). Once the reactor temperature fell below 200ºC, the needle valve at the gas mixture outlet was opened, allowing the reaction gases to pass through a water vapor condenser into a gas sampling bag. The collected gas sample was analyzed by gas chromatography (GC–TCD/FID) to determine its composition. The next test began with flushing the reactor with helium.

Analysis of Gases from Methanation

The analysis of gaseous mixtures from methanation experiments was carried out using a Hewlett Packard 6890 gas chromatograph equipped with a flame ionization detector (FID) and a thermal conductivity detector (TCD).

The TCD channel was used for the determination of permanent gases, including hydrogen. A Haysep Q pre–column was installed at the beginning of the TCD channel to provide a coarse separation of permanent

gases and methane from heavier hydrocarbons (which are retained on the column). This channel also included a Poraplot Q column (30 m in length, 530 μm inner diameter, 50 μm film thickness), used for the separation of CO_2 from a mixture of O_2, N_2, CH_4 and CO. A capillary column with the Poraplot 5A molecular sieve (30 m length, 530 μm in diameter, 50 μm in film thickness) was used to separate permanent gases from methane.

Hydrocarbons (from methane to heptane) were analyzed on the FID channel, equipped with a Restek RT–Alumina BOND/MPD capillary column (30 m length, 0.320 μm inner diameter, 5 μm film thickness).

The split injection ratio was 1:20. The temperature program for the analysis was as follows: i) 70ºC for 7 min; ii) ramp at 10ºC min^{-1} to 90ºC; iii) ramp at 20ºC min^{-1} to 220ºC; iv) hold at 220ºC for 7 min. Helium was used as the carrier gas in both channels.

For qualitative and quantitative chromatographic determination of individual components, several certified reference gas mixtures were used. These contained hydrogen, methane, nitrogen, oxygen, carbon monoxide, carbon dioxide, ethane, ethene, propane, and other hydrocarbons in known concentrations.

Results and Discussion

Properties of Adsorbent/Catalysts

Elemental Analysis

The composition of selected adsorbents before impregnation and adsorbent/catalysts after impregnation is given in Table 1.

Elemental analysis showed a significant decrease in the carbon content of the Envisorb B+ material after its impregnation and the subsequent conversion of the impregnating agent to NiO. This corresponds to the fact that during the impregnation process, black dust of activated carbon was released while the Envisorb B+ adsorbent was mixed with the impregnating solution.

During the activation of Envisorb B+ impregnated with $Ni(NO_3)_2$ (heating to 400ºC), a reaction also occurred between the carbon present in the adsorbent and NO_2 released during the thermal decomposition of nickel nitrate, leading to the removal of a portion of the carbon from the porous structure of the adsorbent. This reaction already proceeds according to the following equation at temperatures above 100ºC [52, 53]:

$$2\ NO_2 + 4\ C \rightarrow N_2 + 4\ CO \qquad (2)$$

Nickel Content and Properties of the Porous Structure of the Materials

The nickel content in the adsorbent/catalyst samples was determined according to the procedure described in the section Determination of nickel content. The BET surface areas and adsorption pore volumes were determined using the method described in the section Determination of BET surface area and pore volume. The specific values characterizing the catalytic and adsorption properties of the tested adsorbents before impregnation and of the adsorbent/catalysts after impregnation are given in Table 2.

In the case of the adsorbent/catalyst based on γ–alumina, a significantly higher Ni concentration was achieved compared to the material based on the Envisorb B+ sorbent. We believe this to be because during the subsequent calcination of the material

Table 1. Elemental composition of adsorbents and adsorbent/catalysts.

adsorbent	Mass fraction (%)			
	N_2	C	H_2	S
γ–alumina	<0.01	0.14	0.49	<0.01
γ–alumina + NiO	<0.01	0.18	0.48	<0.01
Envisorb B+	0.04	15.09	0.78	0.04
Envisorb B+ + NiO	0.02	0.12	0.35	0.03

Table 2. Adsorption properties of adsorbents and adsorbent/catalysts.

adsorbent	NiO content (%)	BET surface area ($m^2\ g^{-1}$)	Adsorption pore volume ($ml\ g^{-1}$)
γ–alumina	–	225	0.462
γ–alumina + NiO	32.4	131	0.250
Envisorb B+	–	565	0.761
Envisorb B+ + NiO	4.2	613	0.742

in a muffle furnace, Ni reacted with the carbon contained in the sorbent, forming volatile nickel tetracarbonyl.

Impregnation of the sorbents with the catalytically active element led to changes in the porous structure of the carriers used. The distribution of pore sizes in the γ–alumina adsorbent before and after impregnation with NiO is shown in Fig. 3, and for the adsorbent based on the Envisorb B+ material in Fig. 4.

It is evident that impregnation of the adsorbents with NiO leads to a significant decrease in both the BET surface area and the pore volume for the γ–alumina–based adsorbent. In the case of the Envisorb B+ adsorbent, no noticeable reduction in these parameters was observed. During impregnation and subsequent thermal treatment, this material experienced a substantial decrease in carbon content and the release of additional pores within its porous structure. This compensated for the pore losses caused by the incorporation of Ni into the porous framework of the adsorbent.

The deposition of nickel particles within the porous structure of the adsorbent leads to a reduction in pore volume, in which CO_2 adsorption takes place. At the same time, nickel enables the methanization of adsorbed CO_2 directly within the pores of the adsorbent/catalyst.

The adsorption capacities of the adsorbent/catalysts for CO_2 at various temperatures were determined according to the procedure described in the section Determination of CO_2 Sorption Capacity. The adsorption capacities of the adsorbent/catalysts are summarized in Table 3.

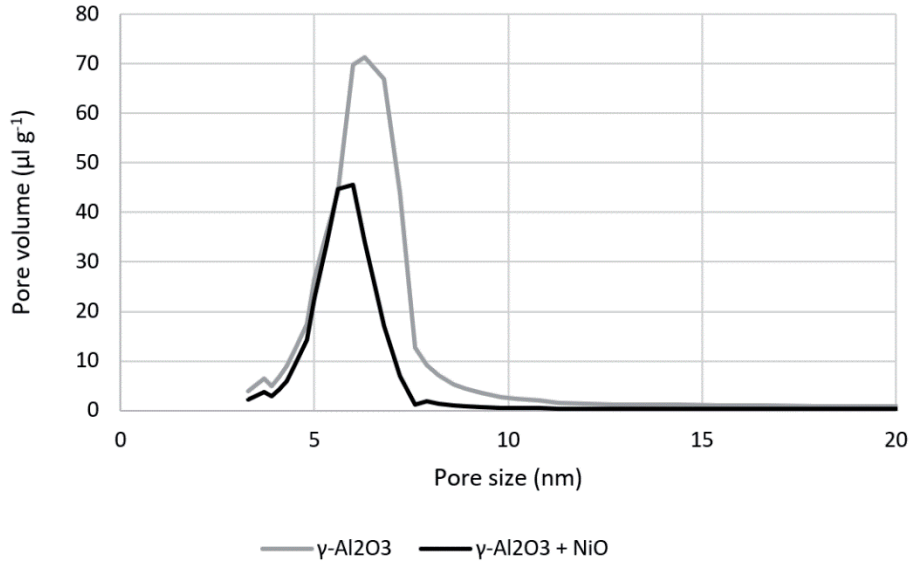


Fig. 3. Pore size distribution of γ–Al_2O_3 before and after NiO impregnation.

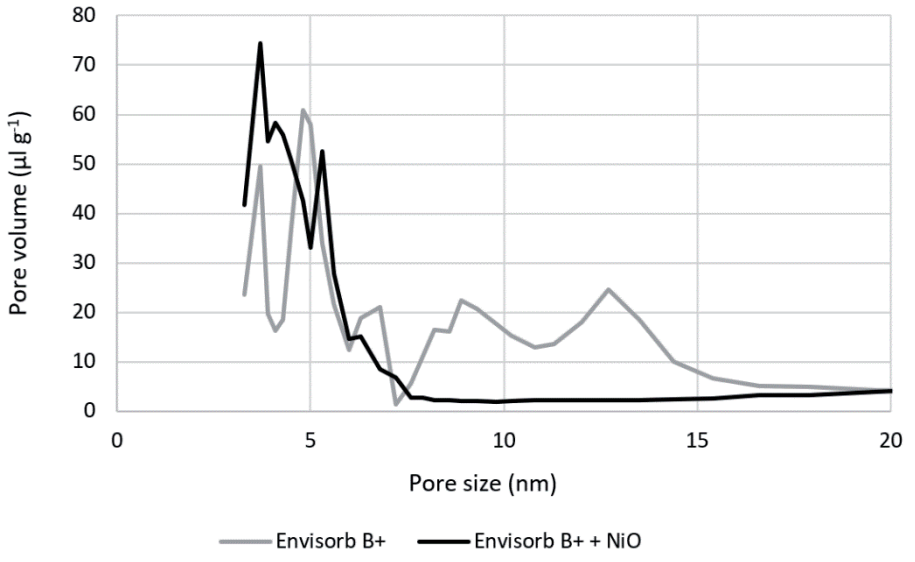


Fig. 4. Pore size distribution of Envisorb B+ before and after NiO impregnation.

Table 3. Adsorption capacities of the adsorbent/catalysts for CO_2.

	Adsorption capacity for CO_2 (g CO_2 per 100 g of adsorbent/catalyst)			
	t = 40ºC	t = 60ºC	t = 80ºC	t = 100ºC
γ–alumina + NiO	0.34	0.28	0.18	0.15
Envisorb B+ + NiO	0.36	0.23	0.18	0.12

The results clearly show that with increasing adsorption temperature, the CO_2 adsorption capacity of both adsorbent/catalysts decreased. Both adsorbents capture CO_2 under the given conditions based on the principle of physical adsorption, which allows their regeneration by increasing the temperature through thermal desorption (TSA). It is also evident that despite their different compositions (polarity) and differing porous structure properties, their CO_2 adsorption capacities under the same conditions are similar.

Methanation

Methanation of CO_2 in static reactors remains a relatively underexplored area; therefore, it was necessary to test a wide range of reaction conditions (temperature, reaction time) to achieve the highest possible conversion of carbon dioxide to methane. Methanation tests with the adsorbent/catalyst based on γ–Al_2O_3 were conducted under the conditions listed in Table 4.

According to the concentration of methane in the outlet gases after the methanation tests using a γ–Al_2O_3–based adsorbent/catalyst, it is evident that methanation took place in tests at temperatures ranging from 500ºC to 330ºC (310ºC only very weakly), while a higher temperature and a long reaction time (21 h) had negative effects on the methane content in the gas. However, at 330ºC, the methane content in the gas increased with a longer reaction time.

Methanation tests with the Envisorb B+–based adsorbent/catalyst were performed only after the methanation experiments were completed with the γ–Al_2O_3–based adsorbent/catalyst. Therefore, the reaction conditions for these tests were adjusted based on the results obtained from the γ–Al_2O_3–based system. The specific conditions of the methanation tests using the Envisorb B+–based adsorbent/catalyst are summarized in Table 5.

Table 4. Conditions of methanation tests with the adsorbent/catalyst based on γ–Al_2O_3.

Methanation Temperature (ºC)	Heating time at target temperature	Before heating		Composition of the gas sample taken after methanation		
		p (CO_2) (MPa)	p (H_2) (MPa)	x (CH_4) (%)	x (CO_2) (%)	x (H_2) (%)
500	0 h*	0.02	1.01	28.6	21.7	46.8
500	0 h*	0.05	1.05	16.6	21.3	55.4
500	21 h	0.02	1.05	1.0	57.3	40.5
470	0 h*	0.02	1.01	27.4	2.9	68.3
450	0 h*	0.02	1.01	25.0	3.9	69.1
430	0 h*	0.05	1.01	25.3	10.4	62.3
410	0 h*	0.05	1.02	21.7	8.6	68.0
390	0 h*	0.05	1.01	19.1	10.4	68.7
370	0 h*	0.05	1.01	12.6	11.8	74.2
350	0 h*	0.05	1.01	13.7	14.7	70.2
330	0 h*	0.05	1.01	12.1	13.3	73.2
310	0 h*	0.05	1.01	5.1	14.8	79.8
330	3 h	0.05	1.01	38.7	4.7	54.8
330	6 h	0.05	1.01	41.3	3.4	54.3
330	12 h	0.05	1.01	48.5	3.5	46.4

Note: * The reactor heating was turned off immediately after reaching the desired methanation temperature.

Table 5. Conditions of methanation tests with the adsorbent/catalyst based on Envisorb B+.

Methanation Temperature/ºC	Heating time at target temperature	Before heating		Composition of the gas sample taken after methanation		
		p (CO_2)/MPa	p (H_2)/MPa	x (CH_4)/%	x (CO_2)/%	x (H_2)/%
490	0 h	0.05	1.01	0.0	22.7	76.8
470	16 h	0.05	1.01	0.5	23.3	75.7
410	0 h	0.05	1.01	0.0	36.8	63.0
350	3 h	0.05	1.00	24.2	52.3	22.7
330	0 h	0.05	1.03	detected	26.6	72.5
350	3 h	0.02	1.51	29.2	20.2	49.6
350	6 h	0.02	1.51	39.2	21.2	38.0
350	12 h	0.02	1.50	46.1	23.5	29.2
350	14 h	0.02	1.51	29.6	1.0	68.4
345	3 h	0.05	1.51	14.0	28.0	55.9
340	6 h	0.02	1.50	22.6	22.1	53.9
330	3 h	0.03	1.50	9.5	21.4	68.2

The results show that the methanation reaction in the Envisorb B+ adsorbent/catalyst proceeds efficiently at temperatures between 330ºC and 350ºC. At higher temperatures, the efficiency of methanation decreases, probably due to the reverse reaction leading to the decomposition of methane in the presence of water vapor. At temperatures below 330ºC, the methanation rate is low, resulting in low methane yields.

Based on the determined concentrations of the main gaseous components (CH_4, CO_2 and H_2) in the gas samples collected after the methanation experiments, the conversion of CO_2 to methane was calculated using the following equation:

$$Y_{CO2} = 100 \times x_{CH4} / (x_{CH4} + x_{CO2}) \quad (3)$$

where:

Y_{CO2} – conversion of CO_2 to CH_4 (%)

x_{CH4} – methane fraction in the gas mixture after methanation (%)

x_{CO2} – carbon dioxide fraction in the gas mixture after methanation (%)

The conversion of CO_2 to CH_4 in the produced gas mixture as a function of reactor temperature in experiments where the reactor heating was switched off immediately after reaching the target temperature is shown in Fig. 5.

The effect of the reaction time on the conversion of CO_2 to methane at 330ºC for the γ–Al_2O_3–based material is shown in the Fig. 6.

It is evident that the reaction time also significantly affects the conversion of CO_2 to CH_4. To achieve operationally acceptable CO_2–to–CH_4 conversions with the Ni catalyst supported on γ–Al_2O_3 in a batch reactor, a reaction time of at least 3 h is required. At short reaction times – when the reactor heating

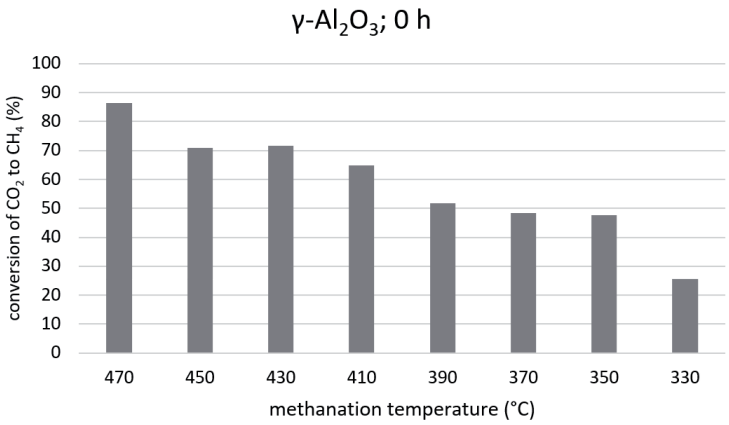


Fig. 5. Effect of reaction temperature on the conversion of carbon dioxide to methane (γ–Al_2O_3, heating switched off when the target temperature was reached).

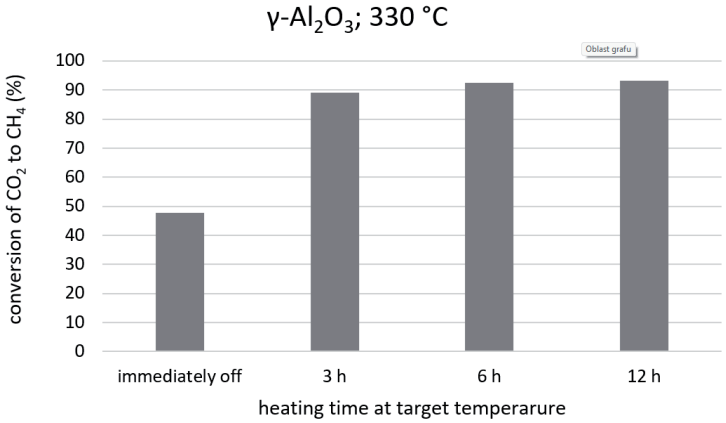


Fig. 6. Effect of reaction time on the conversion of carbon dioxide to methane (γ–Al_2O_3, heating time at target temperature: 330ºC).

is turned off immediately after reaching the target methanation temperature and the gas mixture is released from the reactor – the CO_2 conversion to CH_4 is approximately half that observed at longer reaction times.

Methanation experiments conducted with the Envisorb B+–based material did not yield such clear results. The effect of temperature on CO_2–to–CH_4 conversion over this catalyst is shown in Fig. 7.

The effect of reaction time on the conversion of CO_2 to CH_4 on the Envisorb B+–based catalyst at a temperature of 350ºC is shown in the Fig. 8.

Table 6 presents the properties of the materials tested before and after the methanation experiments.

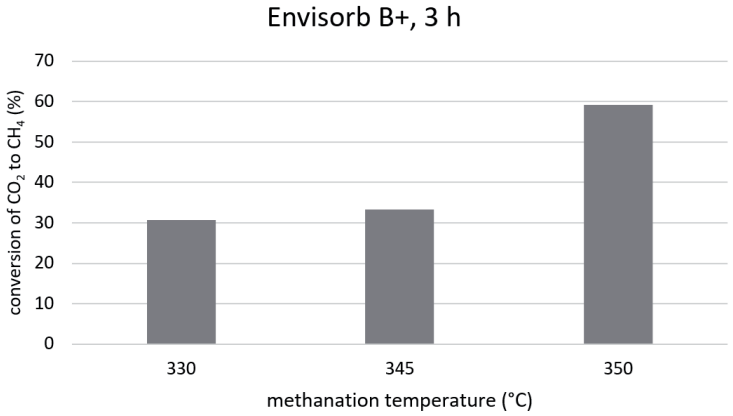


Fig. 7. Effect of reaction temperature on the conversion of carbon dioxide to methane (Envisorb B+, 3 h of heating at the target temperature).

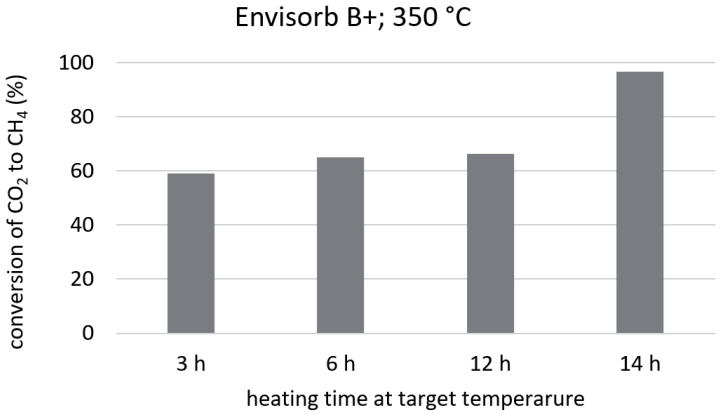


Fig. 8. Effect of reaction time on the conversion of carbon dioxide to methane (Envisorb B+, heating time at target temperature: 350ºC).

Table 6. Properties of the adsorbent/catalyst materials before and after the methanation tests.

		γ–Al_2O_3 + NiO	Envisorb B+ + NiO
NiO content – before the experiments (%)		32.4	4.2
NiO content – after the experiments (%)		33.3	9.8
Specific surface area – before the experiments (m^2 g^{-1})		131	613
Specific surface area – after the experiments (m^2 g^{-1})		90	425
Pore volume – before experiments (ml g^{-1})		0.250	0.742
Pore volume – after experiments (ml g^{-1})		0.256	0.700
Elemental composition – before experiments (% wt.)	N	< 0.01	0.02
	C	0.18	0.12
	H	0.48	0.35
	S	< 0.01	0.03
Elemental composition – after experiments (% wt.)	N	< 0.01	< 0.01
	C	0.19	0.16
	H	0.39	0.31
	S	< 0.01	0.07

Analyses of the adsorbents/catalysts after the experiments, compared with measurements of the same parameters before the tests, showed a slight carbon deposition within the porous structure of both materials. This resulted in a decrease in the specific surface area by approximately 30%. The deactivation of both catalysts likely contributed to the observed decline in their reactivity [54, 55].

The observed conversion of CO_2 to methane may be partly attributed to the relatively large noncatalytic gas volume of the reaction system. Due to the small dimensions of the laboratory reactor, a considerable fraction of the total gas volume is located outside the heated catalytic bed, including connecting tubing, the pressure gauge, and the safety valve. These parts of the apparatus are not filled with the catalyst/adsorbent and are not heated to the reaction temperature.

Since no forced gas flow was present in the static reactor, gas exchange between these nonheated dead volumes and the heated catalytic bed is expected to be limited by mass transfer. As a result, part of the gas may be exchanged only slowly with the catalytic zone during the experiment. At the end of the experiment, however, the gas from the entire system, including both the reactor and the non-reactor volumes, was released into the collection vessel and analyzed together. This may lead to an underestimation of the conversion achieved within the heated catalytic bed itself. The volume distribution of the reaction system is summarized in Table 7.

The gas-filled volume of the system containing the catalyst/adsorbent represents only part of the total reaction system volume, while a substantial fraction corresponds to non-catalytic dead volume (39%). This limitation is mainly related to the small scale of the laboratory apparatus and is expected to become less significant in larger-scale reactors, where the ratio between the catalytic bed volume and the external dead volume is more favorable.

The results presented in this article were compared with similar findings reported in the scientific literature, and a high degree of agreement with the literature data was found. The negative effect of water formed during the methanation reaction on the reaction equilibrium at higher temperatures appears to be particularly significant [58-60].

Table 7. Volume distribution of the laboratory static methanation system and contribution of non-catalytic dead volume.

Reaction system volume determined using He	147.7 ml
Reaction system volume filled with Envisorb B+	131.2 ml
Geometric reactor volume (from dimensions: diameter 30 mm, length 150 mm)	106 ml
Geometric volume of the reactor reduced by the volume of the adsorbent	89.5 ml
Reactor contribution to the total volume of the reaction system	61 %
Contribution of non–reactor spaces	39 %

Conclusions

Experimental tests of catalytic methanation of carbon dioxide with hydrogen in a batch laboratory reactor using catalysts based on γ–Al_2O_3 or Envisorb B+ confirmed the suitability of this technology for capturing CO_2 from gas mixtures and subsequently converting it to methane in a single reactor using one material.

The results obtained during the testing of both catalytically active materials clearly show that, unlike methanation in a flow reactor, where the residence time of the gas mixture is only a few seconds, CO_2 methanation in a batch reactor proceeds significantly more slowly. The methanation rate in this case is likely influenced by the diffusivity of the reacting components in the static reactor, where no gas flow occurs. Under short reaction times and low reactor temperatures, only moderate levels of CO_2–to–CH_4 conversion ranging from 26 to 65 % were achieved, using γ–Al_2O_3 impregnated with Ni. Higher conversion levels were obtained at elevated reaction temperatures, where the methanation reaction proceeds more rapidly (up to a maximum of 90% at 470ºC). At low reactor temperatures (330ºC), the CO_2 to CH_4 conversion can be increased by extending the reaction time. A CO_2 conversion of 93% was achieved at a reactor temperature of 330ºC with a reaction time of 12 h. Similar results were also observed during the testing of Envisorb B+. This suggests that in the static reactor, all processes affecting the rate of the methanation reaction proceed significantly more slowly than in a flow-through reactor. The likely cause is the slow diffusion of gas components in the static environment with high pressure (high gas density).

The apparent carbon dioxide conversion in the laboratory static reactor was likely affected by the relatively large non-heated and non-catalytic dead volume of the reaction system. The limitation of the apparatus may have slowed gas exchange with the heated catalytic bed and contributed to a lower apparent conversion calculated from the final gas composition. In larger-scale reactors, this effect is expected to be less pronounced due to a more favorable ratio between the catalytic bed volume and the external dead volume.

Acknowledgments

This work was supported by the Technology Agency of the Czech Republic (grant number TK05020077 "System for obtaining carbon dioxide from flue gases usable for the production of synthetic methane and other fuels").

Conflict of Interest

The authors declare no conflict of interest.

AI Usage Disclosure Statement

During the preparation of this work, the authors used ChatGPT-5.1 solely for the translation of the manuscript into English. The tool was not used for data generation, data analysis, interpretation of results, or scientific content creation. After using this tool, the authors reviewed and edited the content as needed and assume full responsibility for the content of the published article.

References

1. Directive 2009/31/EC of the European Parliament and of the Council of 23 April 2009 on the Geological Storage of Carbon Dioxide and amending Council Directive 85/337/EEC, Directives 2000/60/EC, 2001/80/EC, 2004/35/EC, 2006/12/EC and 2008/1/EC of the European Parliament and of the Council, and Regulation (EC) No 1013/2006
2. MARWOOD M., DOEPPER R., RENKEN A. *In-situ* surface and gas phase analysis for kinetic studies under transient conditions: The catalytic hydrogenation of CO_2. Applied Catalysis A: General, **151** (1), 223, **1997**.
3. AZIZ M.A.A., JALIL A.A., TRIWAHYONO S., MUKTI R.R., TAUFIQ-YAP Y.H., SAZEGAR M.R. Highly active Ni-promoted mesostructured silica nanoparticles for CO_2 methanation. Applied Catalysis B: Environmental, **147**, 359, **2014**.
4. CHOE S.-J., KANG H.-J., KIM S.-J., PARK S.-B., PARK D.-H., HUH D.-S. Adsorbed Carbon Formation and Carbon Hydrogenation for CO_2 Methanation on the Ni(111)Surface ASED-MO Study. Bulletin of the Korean Chemical Society, **26** (11), 1682, **2005**.
5. SCHILD C., WOKAUN A., BAIKER A. On the mechanism of CO and CO_2 hydrogenation reactions on zirconia-supported catalysts: A diffuse reflectance FTIR study Part I. Identification of surface species and methanation reactions on palladium/zirconia catalysts. Journal of Molecular Catalysis, **63** (2), 223, 1990.
6. ŠNAJDROVÁ V., HLINČÍK T., JÍLKOVÁ L., VRBOVÁ V., CIAHOTNÝ K. The synthesis of the catalysts for the methanation reaction. Paliva, **9** (4), 99, **2017** [In Czech].
7. ZAMANI A.H., ALI R., BAKAR W.A. The investigation of Ru/Mn/Cu–Al_2O_3 oxide catalysts for CO_2/H_2 methanation in natural gas. Journal of the Taiwan Institute of Chemical Engineers, **45** (1), 143, **2014**.
8. SHEN C., LIU M., HE S., ZHAO H., LIU C. Advances in the studies of the supported ruthenium catalysts for CO_2 methanation. Chinese Journal of Catalysis, **63**, 1, **2024**.
9. ZHANG L., LI Z., GAO Y., LI Q., DENG Z., MIAO B., HE H., KOK POH C., ZHANG L., HWA CHAN S. Recent advances in supported metal catalysts for CO_2 methanation: mechanisms, materials design, and the promise of perovskite-based supports. Energy Conversion and Management: X, **27**, 101066, **2025**.
10. ZHANG D., ZHANG J., LI R., CHEN H., HAO Q., BAI Y., SHANG J., ZHANG L., MA X. Coal char supported Ni catalysts prepared for CO_2 methanation by hydrogenation. International Journal of Hydrogen Energy, **48** (39), 14608, **2023**.
11. WANG K., MEN Y., LIU S., WANG J., LI Y., TANG Y., LI Z., AN W., PAN X., LI L. Decoupling the size and

support/metal loadings effect of Ni/SiO_2 catalysts for CO_2 methanation. Fuel, **304**, 121388, **2021**.
12. JACQUEMIN M., BEULS A., RUIZ P. Catalytic production of methane from CO_2 and H_2 at low temperature: Insight on the reaction mechanism. Catalysis Today, **157** (1-4), 462, **2010**.
13. SHARMA S., HU Z., ZHANG P., McFARLAND E.W., METIU H. CO_2 methanation on Ru-doped ceria. Journal of Catalysis, **278** (2), 297, **2011**.
14. WANG W., GONG J. Methanation of carbon dioxide: an overview. Frontiers of Chemical Science and Engineering, **5** (1), 2, **2011**.
15. MILLS G.A., STEFFGEN F.W. Catalytic Methanation. Catalysis Reviews, **8** (1), 159, **1974**.
16. BERMEJO-LÓPEZ A., PEREDA-AYO B., GONZÁLEZ-MARCOS J.A., GONZÁLEZ-VELASCO J.R. Alternate cycles of CO_2 storage and in situ hydrogenation to CH_4 on Ni–Na_2CO_3/Al_2O_3: influence of promoter addition and calcination temperature. Sustainable Energy & Fuels, **5** (4), 1194, **2021**.
17. CHEN L., LIU D., WEI G. Performance of Na-Ru/Al_2O_3 dual function material for integrated CO_2 capture and methanation with the presence of coal ashes. Energy Conversion and Management, **299**, 117811, **2024**.
18. JEONG-POTTER C., ZANGIABADI A., FARRAUTO R. Extended aging of Ru-Ni, Na_2O/Al_2O_3 dual function materials (DFM) for combined capture and subsequent catalytic methanation of CO_2 from power plant flue gas. Fuel, **328**, 125283, **2022**.
19. JO S.B., WOO J.H., LEE J.H., KIM T.Y., KANG H.I., LEE S.C., KIM J.C. A novel integrated CO_2 capture and direct methanation process using Ni/CaO catal–sorbents. Sustainable Energy & Fuels, **4** (9), 4679, **2020**.
20. JOMJAREE T., SINTUYA P., SRIFA A., KOO-AMORNPATTANA W., KIATPHUENGPORN S., ASSABUMRUNGRAT S., SUDOH M., WATANABE R., FUKUHARA C., RATCHAHAT S. Catalytic performance of Ni catalysts supported on CeO_2 with different morphologies for low-temperature CO_2 methanation. Catalysis Today, **375**, 234, **2021**.
21. LI L., ZHANG Y., FENG J., ZHAO S., LI K., HUANG Z., LIN H. Ni–Ca–Al Synergistic Effect in Dual-Function Materials for Integrated CO_2 Capture and Conversion. ACS Sustainable Chemistry & Engineering, **12** (2), 925, **2024**.
22. LU B., FAN Y., ZHI X., HAN Z., WU F., LI X., LUO C., ZHANG L. Material design and prospect of dual–functional materials for integrated carbon dioxide capture and conversion. Carbon Capture Science & Technology, **12**, 100207, **2024**.
23. MOHD RIDZUAN N.D., SHAHARUN M.S., ANAWAR M.A., UD-DIN I. Ni–Based Catalyst for Carbon Dioxide Methanation: A Review on Performance and Progress. Catalysts, **12** (5), 469, **2022**.
24. PROAÑO L., ARELLANO-TREVIÑO M.A., FARRAUTO R.J., FIGUEREDO M., JEONG-POTTER C., COBO M. Mechanistic assessment of dual function materials, composed of Ru-Ni, Na_2O/Al_2O_3 and Pt-Ni, Na_2O/Al_2O_3, for CO_2 capture and methanation by in–situ DRIFTS. Applied Surface Science, **533**, 147469, **2020**.
25. SU X., SHEN L. Advances and challenges about Ni–based dual functional materials for alternating cycles of CO_2 storage and in–situ hydrogenation to CH_4. Carbon Capture Science & Technology, **13**, 100278, **2024**.
26. AZIZ M.A.A., JALIL A.A., TRIWAHYONO S., AHMAD A. CO_2 methanation over heterogeneous catalysts recent progress and future prospects. Green Chemistry, **17** (5), 2647, **2015**.
27. GAO J., WANG Y., PING Y., HU D., XU G., GU F., SU F. A thermodynamic analysis of methanation reactions of carbon oxides for the production of synthetic natural gas. RSC Advances, **2** (6), 2358, **2012**.
28. FALCONER J.L., ZAGLI A.E. Adsorption and Methanation of carbon dioxide on a nickel/silica catalyst. Journal of Catalysis, **62** (2), 280, **1980**.
29. KYSELOVÁ V., HAVLÍN J., CIAHOTNÝ K. Preparation and Testing of Polyethylenimine-Impregnated Silica Gel for CO_2 Capture. Gels, **10** (6), 360, **2023**.
30. KHOSROWSHAHI M.S., AGHAJARI A.A., RAHIMI M., MALEKI F., GHIYABI E., REZANEZHAD A., BAKHSHI A., SALARI E., SHAYESTEH H., MOHAMMADI H. Recent progress on advanced solid adsorbents for CO_2 capture: From mechanism to machine learning. Materials Today Sustainability, **27**, 100900, **2024**.
31. DENG H., LI T., LI H., DANG A., HAN Y. Carbon–based adsorbents for CO_2 capture: A systematic review. Journal of Industrial and Engineering Chemistry, **147**, 39, **2025**.
32. SHI W., YU J., LIU H., GAO D., YUAN A., CHANG B. Hierarchically Nanoporous Carbon for CO_2 Capture and Separation: Roles of Morphology, Porosity, and Surface Chemistry. ACS Applied Nano Materials, **6** (9), 7887, **2023**.
33. MASSA F., COPPOLA A., SCALA F. A thermodynamic study of sorption–enhanced CO_2 methanation at low pressure. Journal of CO_2 Utilization, **35**, 176, **2020**.
34. LV Z., DENG T., GAO C., ZHENG Y., WU C., RAN J., QIN C. Promotion of active H–assisted $CaCO_3$ conversion for integrated CO_2 capture and methanation. Chemical Engineering Journal, **489**, 151427, **2024**.
35. GUO Z., BIAN X., DU Y., ZHANG W., YAO D., YANG H. Recent advances in integrated carbon dioxide capture and methanation technology. Journal of Fuel Chemistry and Technology, **51** (3), 293, **2023**.
36. CHEN J., XU Y., LIAO P., WANG H., ZHOU H. Recent Progress in Integrated CO_2 Capture and Conversion Process Using Dual Function Materials: A State–of–the–Art Review. Carbon Capture Science & Technology, **4**, 100052, **2022**.
37. ZHANG K., WANG R. A critical review on new and efficient adsorbents for CO_2 capture. Chemical Engineering Journal, **485,** 149495, **2024**.
38. TSIOTSIAS A.I., CHARISIOU N.D., YENTEKAKIS I.V., GOULA M.A. Capture and methanation of CO_2 using dual-function materials (DFMs). Chemistry Proceedings, **2** (1), 35, **2020**.
39. TSIOTSIAS A.I., CHARISIOU N.D., YENTEKAKIS I.V., GOULA M.A. The role of alkali and alkaline earth metals in the CO_2 methanation reaction and the combined capture and methanation of CO_2. Catalysts, **10** (7), 812, **2020**.
40. FATAH A., MAHMUD H.B., BENNOUR Z., GHOLAMI R., HOSSAIN M. The impact of supercritical CO_2 on the pore structure and storage capacity of shales. Journal of Natural Gas Science and Engineering, **98**, 104394, **2022**.
41. ARI B., SUNOL A.K., SAHINER N. Highly re-usable porous carbon-based particles as adsorbents for the development of CO_2 capture technologies. Journal of CO_2 Utilization, **82**, 102767, **2024**.
42. KIM T., KIM K., LEE G., SEO M., HWANG J. Guidelines for the Design of Solid CO_2 Adsorbents for Mobile Carbon Capture in Heavy-Duty Vehicles: A Review. Korean Journal of Chemical Engineering, **41** (1), 25, **2024**.

43. ZHANG X.G., BUTHIYAPPAN A., JEWARATNAM J., METSELAAR H.S.C., RAMAN A.A.A. Bifunctional materials for integrated CO_2 capture and conversion: review on adsorbent and catalyst types, recent advances, and challenges. Journal of Environmental Chemical Engineering, **12** (1), 111799, **2024**.
44. SWAPNA S., RAMESH A., VENUGOPAL A., MALLESH D., VINOD G., GANGAREDDY K., SHASHIKALA V., PRATHAP C., RADHIKA M. Biomass Waste Turning into Low-Cost Microporous Carbon Adsorbents for Post-Combustion CO_2 Capture. Russian Journal of General Chemistry, **94**, 1179, **2024**.
45. CHUAH C.Y., LI W., YANG Y., BAE T.-H. Evaluation of porous adsorbents for CO_2 capture under humid conditions: The importance of recyclability. Chemical Engineering Journal Advances, **3**, 100021, **2020**.
46. YAPICI E., AKGÜN H., ÖZKAN A., GÜNKAYA Z., BANAR M. An evaluation of carbon–based adsorbents for post–combustion CO_2 capture. International Journal of Global Warming, **29** (3), 265, **2023**.
47. FOORGINEZHAD S., WEILAND F., CHEN Y., HUSSAIN S., JI X. Review and analysis of porous adsorbents for effective CO_2 capture. Renewable & Sustainable Energy Reviews, **215**, 115589, **2025**.
48. ŠKAROHLÍD M. Vliv obsahu CO_2 v palivu na parametry plynového motoru. Paliva, **3,** 111, **2011** [In Czech].
49. VOGT C., MONAI M., KRAMER G.J., WECKHUYSEN B.M. The renaissance of the Sabatier reaction and its applications on Earth and in space. Nature Catalysis, **2**, 188, **2019**.
50. ASHOK J., PATI S., HONGMANOROM P., TIANXI Z., JUNMEI C., KARVI S. A review of recent catalyst advanced in CO_2 methanation processes. Catalysis Today, **356**, 471, **2020**.
51. CHAI K.H., LEONG L.K., WONG D.S.-H., TSAI D.-H., SETHUPATHI S. Effect of CO_2 adsorbents on the Ni-based dual-function materials for CO_2 capturing and in situ methanation. Journal of the Chinese Chemical Society, **67** (6), 998, **2020**.
52. GÖTZ M., LEFEBVRE J., MÖRS F., McDANIEL KOCH A., GRAF F., BAJOHR S., REIMERT R., KOLB T. Renewable Power–to–Gas: a technological and economic review. Renewable Energy, **85**, 1371, **2016**.
53. YOUMAS M., KONG L.L., BASHIR M.J.K., NADEEM H., SHEHZAD A., SETHUPATHI S. Recent advancements, fundamental challenges and opportunities in catalytic methanation of CO_2. Energy & Fuels, **30** (11), 8815, **2016**.
54. BERMEJO-LÓPEZ A., PEREDA-AYO B., GONZÁLEZ-MARCOS J.A., GONZÁLEZ-VELASCO J.R. Ni loading effects on dual function materials for capture and in-situ conversion of CO_2 to CH_4 using CaO or Na_2CO_3. Journal of CO_2 Utilization, **34**, 576, **2019**.
55. MOROSANU E.A., SALOMONE F., PIRONE R., BENSAID S. Insights on a methanation catalyst aging process: aging characterization and kinetic study. Catalysts, **10** (3), 283, **2020**.
56. OLIVEIRA CABRAL T., BELLOT NORONHA F., SOUZA TONIOLO F. Kinetic and DRIFTS studies of the CO_2 catalytic hydrogenation on Ru/SiO_2: A comprehensive and strategic investigation of CO_2 methanation mechanisms by kinetic modeling and data regression. Chemical Engineering Journal, **485**, 149716, **2024**.
57. KOSAKA F., LIU Y., CHEN S.-Y., MOCHIZUKI T., TAKAGI H., URAKAWA A., KURAMOTO K. Enhanced Activity of Integrated CO_2 Capture and Reduction to CH_4 under Pressurized Conditions toward Atmospheric CO_2 Utilization. ACS Sustainable Chemistry & Engineering, **9** (9), 3452, **2021**.
58. CHAMPON I., BENGAOUER A., CHAISE A., THOMAS S., ROGER A.C. Carbon dioxide methanation kinetic model on a commercial Ni/Al_2O_3 catalyst. Journal of CO_2 Utilization, **34**, 256, **2019**.
59. LIM J.Y., McGREGOR J., SEDERMAN A.J., DENNIS J.S. Kinetic studies of CO_2 methanation over Ni/ γ-Al_2O_3 catalyst using a batch reactor. Chemical Engineering Science, **141**, 28, **2016**.
60. ONRUBIA-CALVO J.A., QUINDIMIL A., DAVÓ-QUIÑONERO A., BERMEJO-LÓPEZ A., BAILÓN-GARCÍA E., PEREDA-AYO B., LOZANO-CASTELLÓ D., GONZÁLES-MARCOS J.A., BUENO-LÓPEZ A., GONZÁLES-VELASCO J.R. Kinetics, Model Discrimination, and Parameters Estimation of CO_2 Methanation on Highly Active Ni/CeO_2 Catalyst. Industrial & Engineering Chemistry Research, **61** (29), 10419, **2022**.